Mechanism of Ligand Photodissociation in Photoactivable [Ru(bpy) 2 L 2] 2+ Complexes: A Density Functional Theory Study

5 AUTHORS, INCLUDING:

Luca Salassa
CIC biomaGUNE
86 PUBLICATIONS   1,437 CITATIONS

Giovanni Salassa
University of Geneva
18 PUBLICATIONS   335 CITATIONS

Roberto Gobetto
Università degli Studi di Torino
298 PUBLICATIONS   4,510 CITATIONS

Carlo Nervi
Università degli Studi di Torino
93 PUBLICATIONS   1,483 CITATIONS

Mechanism of Ligand Photodissociation in Photoactivable [Ru(bpy)$_2$L$_2$]$^{2+}$ Complexes: A Density Functional Theory Study

Luca Salassa, Claudio Garino, Giovanni Salassa, Roberto Gobetto,* and Carlo Nervi

Dipartimento di Chimica I.F.M., Università di Torino, Via P. Giuria 7, I-10125 Torino, Italy

Received April 9, 2008; E-mail: roberto.gobetto@unito.it

Abstract: A series of four photodissociable Ru polypyridyl complexes of general formula [Ru(bpy)$_2$L$_2$]$^{2+}$, where bpy = 2,2′-bipyridine and L = 4-aminopyridine (**1**), pyridine (**2**), butylamine (**3**), and γ-aminobutyric acid (**4**), was studied by density functional theory (DFT) and time-dependent density functional theory (TDDFT). DFT calculations (B3LYP/LanL2DZ) were able to predict and elucidate singlet and triplet excited-state properties of **1**−**4** and describe the photodissociation mechanism of one monodentate ligand. All derivatives display a Ru → bpy metal-to-ligand charge transfer (MLCT) absorption band in the visible spectrum and a corresponding emitting triplet ^{3}MLCT state (Ru → bpy). **1**−**4** have three singlet metal-centered (MC) states 0.4 eV above the major ^{1}MLCT states. The energy gap between the MC states and lower-energy MLCT states is significantly diminished by intersystem crossing and consequent triplet formation. Relaxed potential energy surface scans along the Ru−L stretching coordinate were performed on singlet and triplet excited states for all derivatives employing DFT and TDDFT. Excited-state evolution along the reaction coordinate allowed identification and characterization of the triplet state responsible for the photodissociation process in **1**−**4**; moreover, calculation showed that no singlet state is able to cause dissociation of monodentate ligands. Two antibonding MC orbitals contribute to the ^{3}MC state responsible for the release of one of the two monodentate ligands in each complex. Comparison of theoretical triplet excited-state energy diagrams from TDDFT and unrestricted Kohn−Sham data reveals the experimental photodissociation yields as well as other structural and spectroscopic features.

Introduction

Photodissociation of ligands from metal complexes has been extensively studied in a variety of derivatives for synthetic reasons[1,2] since the 1980s.[3,4] Photoreactions are characterized by loss of a monodentate ligand and coordination of a solvent molecule. In nonpolar solvents, the solvent molecule is replaced by coordination of counterions, added ions, or residual water. Photodissociation of a second monodentate ligand is generally more difficult.

Recently, new interest has grown around transition metal complexes that are able to release one of the coordinated ligands when excited with a specific wavelength of light.[5–9] Such attention is motivated by two different but equally appealing applications: first, the light activation of a specific and desired interaction between the metal complex and its biological target,[10–12] and second, the controlled delivery of small, biologically active, organic or inorganic molecules.[6–9,13] In principle, phototriggering allows spatial control of activated species, which may reduce the negative side effects of metals in certain tissues.[14] Tissue damage may be further reduced by using visible light excitation instead of UV light.

Specific and desired interactions between platinum and its biotarget have been successfully realized in medicinal chemistry.[15–17] Sadler et al. synthesized *trans,trans,trans*-[Pt(N$_3$)$_2$-(OH)$_2$(NH$_3$)$_2$] and studied photoactivation effects on its toxicity toward skin cancer cells. This *trans*-platinum(IV) complex is less toxic in the dark, yet it is as cytotoxic as cisplatin when irradiated by UVA light. Since chemotherapeutics of this kind

(1) Adelt, M.; Devenney, M.; Meyer, T. J.; Thompson, D. W.; Treadway, J. A. *Inorg. Chem.* **1998**, *37*, 2616–2617.
(2) Moss, J. A.; Leasure, R. M.; Meyer, T. J. *Inorg. Chem.* **2000**, *39*, 1052–1058.
(3) Pinnick, D. V.; Durham, B. *Inorg. Chem.* **1984**, *23*, 1440–1445.
(4) Balzani, V.; Carassitti, V. *Photochemistry of Coordination Compounds*; Academic Press: New York, 1970.
(5) Petroni, A.; Slep, L. D.; Etchenique, R. *Inorg. Chem.* **2008**, *47*, 951–956.
(6) Zayat, L.; Noval, M. G.; Campi, J.; Calero, C. I.; Calvo, D. J.; Etchenique, R. *ChemBioChem* **2007**, *8*, 2035–2038.
(7) Zayat, L.; Salierno, M.; Etchenique, R. *Inorg. Chem.* **2006**, *45*, 1728–1731.
(8) Nikolenko, V.; Yuste, R.; Zayat, L.; Baraldo, L. M.; Etchenique, R. *Chem. Commun.* **2005**, 1752–1754.
(9) Zayat, L.; Calero, C.; Albores, P.; Baraldo, L.; Etchenique, R. *J. Am. Chem. Soc.* **2003**, *125*, 882–883.
(10) Menon, E. L.; Perera, R.; Navarro, M.; Kuhn, R. J.; Morrison, H. *Inorg. Chem.* **2004**, *43*, 5373–5381.
(11) Morrison, H.; Harmon, H. *Photochem. Photobiol.* **2000**, *72*, 731–738.
(12) Loganathan, D.; Rodriguez, J. H.; Morrison, H. *J. Am. Chem. Soc.* **2003**, *125*, 5640–5641.
(13) Caruso, E. B.; Cicciarella, E.; Sortino, S. *Chem. Commun.* **2007**, 5028–5030.
(14) Gielen, M.; Tiekink, E. *Metallotherapeutic Drugs and Metal-based Diagnostic Agents: The Use of Metals in Medicine*; John Wiley & Sons: Chichester, 2005.
(15) Bednarski, P. J.; Grunert, R.; Zielzki, M.; Wellner, A.; Mackay, F. S.; Sadler, P. J. *Chem. Biol.* **2006**, *13*, 61–67.
(16) Heringova, P.; Woods, J.; Mackay, F. S.; Kasparkova, J.; Sadler, P. J.; Brabec, V. *J. Med. Chem.* **2006**, *49*, 7792–7798.
(17) Mackay, F. S.; Woods, J. A.; Moseley, H.; Ferguson, J.; Dawson, A.; Parsons, S.; Sadler, P. J. *Chem.-Eur. J.* **2006**, *12*, 3155–3161.

lack toxicity in the dark and form active species only when a particular area is irradiated, unpleasant chemotherapy side effects can be reduced by such a new generation of prodrugs.

The study of excited-state properties in coordination chemistry is a cornerstone in the knowledge of light-induced ligand dissociation phenomena, and thus it is essential to the development of new molecules with suitable characteristics for biological applications. Density functional theory (DFT) and time-dependent density functional theory (TDDFT) are potent and efficient tools for excited-state characterization of transition metal complexes.[18–22] Nevertheless, only a limited number of computational studies regarding ligand photodissociation in transition metal complexes have been published. Head-Gordon et al. investigated ultrafast CO dissociation from the CO-ligated iron porphyrin by using TDDFT,[23] while De Angelis et al. explored the photodissociation pathways for O_2 adducts of myoglobin.[24] Vlček et al. studied ultrafast CO photodissociation in $[M(CO)_4(bpy)]$ (where M = Cr, Mo, W and bpy = 2,2′-bipyridine) and $[Ru(X)_2(CO)_2(bpy)]$ (where X = Cl, Br, I) derivatives,[25–28] and Reedijk et al. studied NO dissociation from the cytotoxic *cis*-(Cl,Cl)-[Ru(terpy)(NO)(Cl)₂]Cl complex (where terpy = 2,2′:6′,2″-terpyridine).[29] In all these works, DFT played a crucial role in the characterization of the excited states and in the analysis of spectroscopy results. The presence of a CO and NO ligand offered the dual advantages of having unique spectroscopic features and being computationally less time-demanding compared to other monodentate ligands.

We have been intrigued by the photochemical properties of some $[Ru(bpy)_2(L)_2]^{2+}$ complexes (where L = neuroactive aromatic or aliphatic amine) synthesized and studied by Etchenique and co-workers.[6–9] In a recent paper,[9] the authors studied the *in vitro* photorelease of 4-aminopyridine from the complex $[Ru(bpy)_2(4ap)]^{2+}$ (where 4ap = 4-aminopyridine) upon excitation with 490-nm light and the induced effect on cellular membrane potential using neurophysiological techniques. Furthermore, $[Ru(bpy)_2(L)_2]^{2+}$ complexes have shown potential as anticancer drugs,[30,31] and it was also demonstrated that the derivative $[Ru(bpy)_2(NH_3)_2]^{2+}$ has DNA-binding properties dependent on photoactivation.[31]

In this paper we report our DFT and TDDFT studies on a series of photoactivable $[Ru(bpy)_2(L)_2]^{2+}$ complexes that showed interesting photochemical features. The four selected complexes coordinate the following amines as monodentate ligands (L): **1**, 4-aminopyridine (4ap); **2**, pyridine (py); **3**, butylamine (a-but); and **4**, γ-aminobutyric acid (gaba). Although ligand release from this type of complex has been shown (**2** in particular),[3,32] the literature lacks detailed computational studies. We investigated singlet and triplet excited states for all derivatives so that, by identifying and characterizing the states involved in the photochemical process, we could dissect the ligand dissociation mechanism. The detailed knowledge of these aspects of metal complexes' photochemistry can help in the design of efficient photoactivable molecules for several applications in medicinal chemistry.

Computational Details

All calculations were performed with the Gaussian 03 (G03) program package[33] employing the DFT method with Becke's three-parameter hybrid functional[34] and Lee−Yang−Parr's gradient-corrected correlation functional[35] (B3LYP). The LanL2DZ basis set[36] and effective core potential were used for the Ru atom, and the split-valence 6-31G** basis set[37] was applied for all other atoms. The ground-state geometries of the complexes (**S1−4**) were optimized in the gas phase. The lowest-lying triplet state geometries of the four complexes (**T1−4**) were calculated in the gas phase using the unrestricted Kohn−Sham formalism (UKS) with unrestricted B3LYP functional (UB3LYP). Geometry optimization was performed without any constraint, and the nature of all stationary points was confirmed by normal-mode analysis. Electronic structures for **S1−4** and **T1−4** were calculated using the conductor-like polarizable continuum model method (CPCM)[38–40] with water as solvent.

Nonequilibrium TDDFT[41,42] calculations produced singlet and triplet excited states, using the CPCM method with water as solvent. Thirty-two singlet excited states and eight triplet excited states[43,44] were determined starting from **S1−4** geometries; computational results are summarized in Tables 1 and 2. Electronic distributions and localizations of the singlet and triplet excited states were visualized using the electron density difference maps (EDDMs).[45] GaussSum 1.05[46] was used for singlet EDDMs calculations and for simulation of the electronic spectrum. Triplet EDDMs were obtained with GaussView 4.1.2,[47] taking into account all major components and their relative weight.

The ΔSCF approach[18] was used for evaluating emission energies of the complexes. The ΔSCF method calculates the emission energy
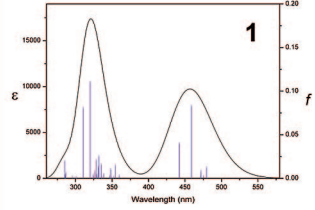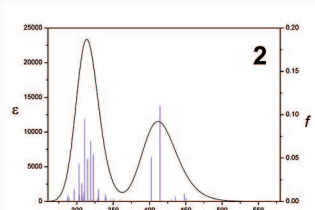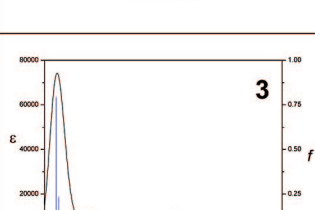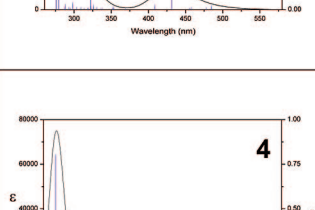
(18) Vlček, A.; Zališ, S. *Coord. Chem. Rev.* **2007**, *251*, 258–287.
(19) De Angelis, F.; Fantacci, S.; Selloni, A.; Nazeeruddin, M. K.; Grätzel, M. *J. Am. Chem. Soc.* **2007**, *129*, 14156–14157.
(20) Di Censo, D.; Fantacci, S.; De Angelis, F.; Klein, C.; Evans, N.; Kalyanasundaram, K.; Bolink, H. J.; Grätzel, M.; Nazeeruddin, M. K. *Inorg. Chem.* **2008**, *47*, 980–989.
(21) Albertino, A.; Garino, C.; Ghiani, S.; Gobetto, R.; Nervi, C.; Salassa, L.; Rosenberg, E.; Sharmin, A.; Viscardi, G.; Buscaino, R.; Croce, G.; Milanesio, M. *J. Organomet. Chem.* **2007**, *692*, 1377–1391.
(22) Garino, C.; Gobetto, R.; Nervi, C.; Salassa, L.; Rosenberg, E.; Ross, J. B. A.; Chu, X.; Hardcastle, K. I.; Sabatini, C. *Inorg. Chem.* **2007**, *46*, 8752–8762.
(23) Dunietz, B. D.; Dreuw, A.; Head-Gordon, M. *J. Phys. Chem. B* **2003**, *107*, 5623–5629.
(24) De Angelis, F.; Car, R.; Spiro, T. G. *J. Am. Chem. Soc.* **2003**, *125*, 15710–15711.
(25) Guillaumont, D.; Vlček, A.; Daniel, C. *J. Phys. Chem. A* **2001**, *105*, 1107–1114.
(26) Vlček, A. *Coord. Chem. Rev.* **2002**, *230*, 225–242.
(27) Vlček, A. *Coord. Chem. Rev.* **1998**, *177*, 219–256.
(28) Gabrielsson, A.; Zališ, S.; Matousek, P.; Towrie, M.; Vlček, A. *Inorg. Chem.* **2004**, *43*, 7380–7388.
(29) Karidi, K.; Garoufis, A.; Tsipis, A.; Hadjiliadis, N.; den Dulk, H.; Reedijk, J. *Dalton Trans.* **2005**, 1176–1187.
(30) Novakova, O.; Kasparkova, J.; Vrana, O.; Vanvliet, P. M.; Reedijk, J.; Brabec, V. *Biochemistry* **1995**, *34*, 12369–12378.
(31) Singh, T. N.; Turro, C. *Inorg. Chem.* **2004**, *43*, 7260–7262.
(32) Demas, J. N.; Degraff, B. A. *Anal. Chem.* **1991**, *63*, A829–A837.
(33) Frisch, M. J. ; et al. *Gaussian 03*, revision D.01; Gaussian Inc.: Wallingford, CT, 2004.
(34) Becke, A. D. *J. Chem. Phys.* **1993**, *98*, 5648–5652.
(35) Lee, C.; Yang, W.; Parr, R. G. *Phys. Rev. B: Condens. Matter* **1988**, *37*, 785–789.
(36) Hay, P. J.; Wadt, W. R. *J. Chem. Phys.* **1985**, *82*, 270–283.
(37) McLean, A. D.; Chandler, G. S. *J. Chem. Phys.* **1980**, *72*, 5639–5648.
(38) Cossi, M.; Rega, N.; Scalmani, G.; Barone, V. *J. Comput. Chem.* **2003**, *24*, 669–681.
(39) Cossi, M.; Barone, V. *J. Chem. Phys.* **2001**, *115*, 4708–4717.
(40) Barone, V.; Cossi, M. *J. Phys. Chem. A* **1998**, *102*, 1995–2001.
(41) Casida, M. E.; Jamorski, C.; Casida, K. C.; Salahub, D. R. *J. Chem. Phys.* **1998**, *108*, 4439–4449.
(42) Stratmann, R. E.; Scuseria, G. E.; Frisch, M. J. *J. Chem. Phys.* **1998**, *109*, 8218–8224.
(43) Villegas, J. M.; Stoyanov, S. R.; Huang, W.; Rillema, P. D. *Inorg. Chem.* **2005**, *44*, 2297–2309.
(44) Stoyanov, S. R.; Villegas, J. M.; Cruz, A. J.; Lockyear, L. L.; Reibenspies, J. H.; Rillema, P. D. *J. Chem. Theory Comput.* **2005**, *1*, 95–106.
(45) Browne, W. R.; O'Boyle, N. M.; McGarvey, J. J.; Vos, J. G. *Chem. Soc. Rev.* **2005**, *34*, 641–663.
(46) O'Boyle, N. M. ; Vos, J. G. *GaussSum 1.0*; Dublin City University: Dublin, Ireland, 2005; available at http://gausssum.sourceforge.net.
(47) Dennington, R., II; Keith, T.; Millam, J. *GaussView4.1*; Semichem, Inc.: Shawnee Mission, KS, 2007.

Table 1. Selected Bond Distances (Å) and Angles (deg) of Complexes **1**−**4** in Calculated Singlet Ground-State (**S1**−**4**) and Lowest-Lying Triplet-State (**T1**−**4**) Geometries[a]

Scheme	Geometry	Ru−N1	Ru−N2	Ru−N3	Ru−N4	Ru−N5	Ru−N6	N1−Ru−N5	N3−Ru−N6
	S1	2.11	2.12	2.10	2.12	2.18	2.18	175.61	175.61
	S2	2.11	2.13	2.11	2.13	2.18	2.18	175.98	175.98
	S3	2.10	2.13	2.10	2.13	2.22	2.22	173.41	173.42
	S4	2.10	2.13	2.10	2.13	2.23	2.23	173.66	173.66
	T1	2.45	2.20	2.12	2.11	2.69	2.17	157.43	174.83
	T2	2.43	2.20	2.12	2.11	2.78	2.17	157.33	174.91
	T3	2.45	2.18	2.12	2.13	2.72	2.23	170.02	173.27
	T4	2.44	2.18	2.12	2.13	2.74	2.23	165.13	173.18

[a] N5, N6 = 4ap (**S1**, **T1**), py (**S2**, **T2**), a-but (**S3**, **T3**), gaba (**S4**, **T4**).

Table 2. Selected Calculated Singlet Excited-State Transitions for Complexes **1**−**4** in Water[a]

Complex	Trans.	Energy	f	Major Contribution	Character
1	1	2.58 (480)	0.012	HOMO→LUMO (54%)	MLLCT
	2	2.61 (475)	0.002	HOMO−2→LUMO+1 (89%)	MLCT
	3	2.63 (472)	0.008	HOMO−2→LUMO (72%)	MLCT
	4	2.63 (471)	0.003	HOMO−1→LUMO (54%)	MLLCT
	5	2.70 (459)	0.082	HOMO−1→LUMO+1 (38%) HOMO→LUMO (40%)	MLLCT
	6	2.80 (442)	0.039	HOMO−1→LUMO(36%) HOMO→LUMO+1 (53%)	MLLCT
	24	3.87 (320)	0.110	HOMO−2→LUMO+5 (82%)	MLCT
	25	3.99 (311)	0.080	No major contribution	MLCT
2	1	2.75 (451)	0.002	HOMO→LUMO+1 (80%)	MLCT
	2	2.77 (448)	0.008	HOMO→LUMO (92%)	MLCT
	3	2.85 (435)	0.004	HOMO−1→LUMO+1 (78%)	MLCT
	4	2.89 (430)	0.001	HOMO−1→LUMO (68%)	MLCT
	5	2.99 (414)	0.109	HOMO−2→LUMO (73%) HOMO−1→LUMO+1 (18%)	MLCT
	6	3.08 (403)	0.050	HOMO−2→LUMO+1 (51%) HOMO−1→LUMO (26%)	MLCT
	15	3.84 (323)	0.053	HOMO−2→LUMO+2 (83%)	MLCT
	17	3.89 (319)	0.068	no major contribution	MLCT
	20	3.99 (311)	0.094	HOMO→LUMO+6(71%)	MLCT
3	1	2.56 (485)	0.014	HOMO→LUMO (94%)	MLCT
	2	2.59 (478)	0.002	HOMO→LUMO+1 (84%)	MLCT
	3	2.71 (458)	0.004	HOMO−1→LUMO+1 (76%)	MLCT
	4	2.72 (455)	0.000	HOMO−1→LUMO (77%)	MLCT
	5	2.87 (432)	0.128	HOMO−2→LUMO (73%)	MLCT
	6	3.03 (408)	0.018	HOMO−2→LUMO+1 (60%)	MLCT
	16	3.85 (322)	0.113	HOMO−1→LUMO+3 (60%) HOMO→LUMO+4 (25%)	MLCT
	27	4.44 (279)	0.227	HOMO−4→LUMO+1 (64%)	π−π*
	28	4.49 (276)	0.789	HOMO−4→LUMO (30%) HOMO−3→LUMO+1 (38%)	π−π*
4	1	2.59 (479)	0.015	HOMO→LUMO (93%)	MLCT
	2	2.63 (472)	0.0020	HOMO→LUMO+1 (83%)	MLCT
	3	2.73 (454)	0.0066	HOMO−1→LUMO+1 (76%)	MLCT
	4	2.75 (450)	0.0004	HOMO−1→LUMO (75%)	MLCT
	5	2.90 (427)	0.1258	HOMO−2→LUMO (74%) HOMO−1→LUMO+1 (17%)	MLCT
	6	3.05 (406)	0.0184	HOMO−2→LUMO+1 (58%) HOMO−1→LUMO (15%) HOMO→LUMO+1 (11%)	MLCT
	16	3.88 (320)	0.1141	HOMO−1→LUMO+3 (50%)	MLCT
	27	4.44 (279)	0.2327	HOMO−4→LUMO+1 (61%)	π−π*
	28	4.49 (276)	0.7962	HOMO−4→LUMO (31%) HOMO−3→LUMO+1 (35%)	π−π*

[a] The simulated UV−vis spectra with the oscillator strength values (shown as vertical bars) were obtained with the program GaussSum 2.1.2.[54]

(S_0−T_1) as the difference between the triplet and singlet states at the triplet geometry. Triplet emission energies were also calculated by TDDFT using **T1**−**4** geometries and the CPCM method.

Ru−L Photodissociation Calculations. The effects of Ru−N(L) bond elongation (where L = 4ap, py, a-but, gaba) on singlet and triplet states were studied by TDDFT and UKS employing **S1**−**4**

and **T1**−**4** geometries, respectively. Starting from the optimized **S1**−**4** equilibrium geometries, a single Ru−N(L) (Ru−N5 according to the scheme in Table 1) bond distance was elongated in the range 2.20−3.05 Å by 0.1 Å increments. Every 0.1 Å, the Ru−N(L) bond was frozen, and the geometry of the molecule was relaxed to a stationary point. Each incremental geometry was then employed

for calculating 32 singlet and 8 triplet excited states by TDDFT at the B3LYP/LanL2DZ (6-31G** for C, N, H, O) level. An analogous procedure was employed for UKS calculations on **T1−4** geometries. The Ru−N(L) bond distance was both shortened and elongated in the range 2.20−3.05 Å by 0.1 Å increments. At each 0.1 Å increment, the Ru−N(L) bond was again frozen, and the complexes' geometries were relaxed to a stationary point at the unrestricted B3LYP/LanL2DZ (6-31G** for C, N, H, O) level.

Results and Discussion

Ground-State and Triplet Geometry Features. Striking differences in Ru−N bond lengths are found by comparing the ground-state (**S1−4**) and triplet (**T1−4**) geometries of complexes **1−4**. In the ground-state geometry, **1−4** display two equal Ru−N(L) distances (see Table 1), while Ru−N(bpy) distances in *trans* to L are slightly shorter than the other Ru−N(bpy) bonds (2.10 and 2.12 Å, respectively). In the **T1−4** geometries, one Ru−N(L) bond distance (Ru−N5 in Table 1) is significantly longer than the other; Ru−N(L) bond lengths are 2.69 and 2.17 Å in **T1**, 2.78 and 2.17 Å in **T2**, 2.72 and 2.23 Å in **T3**, and 2.73 and 2.23 Å in **T4**. The Ru−N1(bpy) distance (*trans* to Ru−N5) is also significantly increased (∼0.35 Å) in **T1−4** with respect to **S1−4**. Moreover, the octahedral disposition of the N atoms around the ruthenium center is highly distorted in the **T1−4** geometries. For example, the N1−Ru−N5 angles (∼157°) are significantly smaller than in the ground-state geometries (∼175°) for **1** and **2**. In **T1** and **T2** geometries, 4ap and py bend downward, rotating the ring toward the bpy ligand. Complexes **3** and **4** are less distorted, but the carbon chain of the monodentate ligand is rotated about 90° with respect to its orientation in the ground state. Bite angles of the chelating ligands play an important role in determining the photophysical properties of ruthenium complexes.[48,49] Decrease in the bite angle usually indicates faster nonradiative decay via metal-centered (MC) states. While **S1−4** have common bpy bite angles that fall in the range 77.7°−77.9°, **T1−4** have one of the two bpy bite angles significantly reduced to 70.7° in **1**, 71.2° in **2**, 71.5° in **3**, and 71.4° in **4**.

Orbital Analysis. The ground-state electronic structures of **1−4** were calculated accounting for the solvent effect of water in the CPCM model.[22,38–40] All four complexes display similar frontier orbitals and orbital energy diagrams, although some differences can be observed, particularly in the case of **1**. In **2−4**, the highest occupied molecular orbital (HOMO) is basically ruthenium-centered (83%), with limited contribution from the two bpy moieties. In **1**, the 4ap ligands play a significant role (32% total), and the metal has a reduced contribution (51%). For all complexes, HOMO−1 and HOMO−2 lie within 0.25 eV from HOMO. In **2−4** they are metal-centered (>82%) like the HOMO. In **1**, HOMO−1 is similar to the HOMO, while HOMO−2 is mainly metal-based (85%). Lower in energy, there is a set of three orbitals with mostly bpy and L character. Only **1** has some metal participation in HOMO−4 and HOMO−5.

The lowest unoccupied molecular orbital (LUMO) is localized on the two bpy's (97%) for all complexes. LUMO+1 is almost degenerate in energy and has similar shapes, while the other unoccupied virtual orbitals, up to LUMO+5, are all ligand-
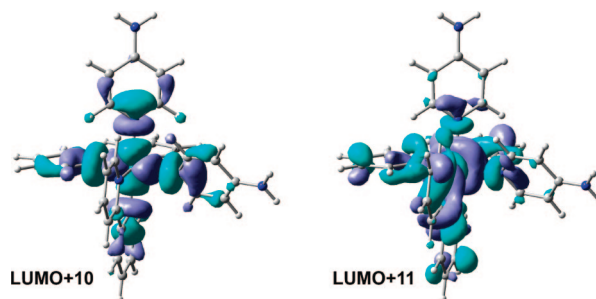
(48) Abrahamsson, M.; Becker, H. C.; Hammarstrom, L.; Bonnefous, C.; Chamchoumis, C.; Thummel, R. P. *Inorg. Chem.* **2007**, *46*, 10354–10364.

(49) Farrell, I. R.; Matousek, P.; Towrie, M.; Parker, A. W.; Grills, D. C.; George, M. W.; Vlček, A. *Inorg. Chem.* **2002**, *17*, 4318–4323.

Figure 1. Isodensity plots (isovalue = 0.02) of the two antibonding molecular orbitals in complex **1**.
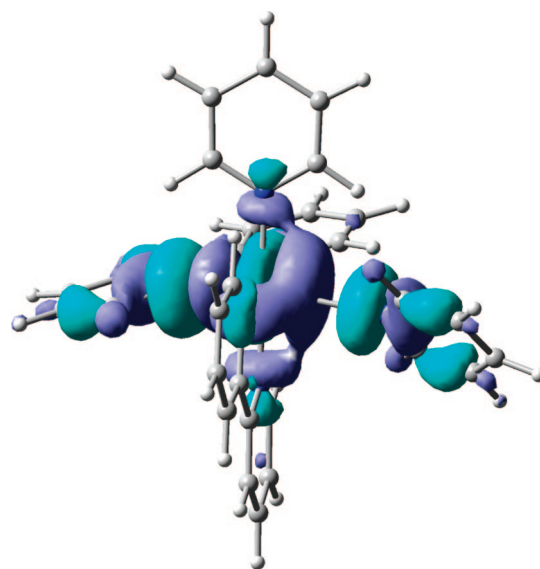

Figure 2. Isodensity plot (isovalue = 0.02) of the higher-energy SOMO in complex **2**.

based, with or without contributions from the monodentate ligands. LUMO+10 and LUMO+11 for **1** and **2**, and LUMO+6 and LUMO+7 for **3** and **4** (Figure 1), are metal-based (60−70%) and have σ-antibonding character toward bpy and L, which contribute 18−34% (**1**, **2**) and 6−20% (**3**, **4**). This set of orbitals is 2.11−2.31 eV above the LUMO and plays an important role in the photodissociation mechanism of the monodentate ligands (see below).

The solvated electronic structures of **T1−4** show relevant differences in frontier orbitals compared to **S1−4**. In fact, the two singly occupied molecular orbitals (SOMOs) do not correspond to the HOMOs and LUMOs of the ground-state geometry. The low-energy SOMO is L-based in **1** and **4** but metal- and bpy-based in **2** and **3**; the high-energy SOMO is metal-based with a strong σ-antibonding character toward the monodentate ligand with the longest Ru−N(L) bond (particularly in **2**, Figure 2) and the bpy ring *trans* to it. Population of the high-energy SOMO causes an increase in both distances. The energy difference between the two SOMOs is 0.85 eV in **1**, 1.46 eV in **2**, 1.59 eV in **3**, and 0.56 eV in **4**. The first empty orbital is at least 1.9 eV over the high-energy SOMO for all complexes.

Absorption Properties and Singlet Excited States of Complexes 1−4. The experimental absorption spectra[7,9] of **1−4** present three major bands that are well reproduced by TDDFT calculations, particularly for **3** and **4**. The lowest-energy bands at 450−480 nm are ¹MLCT states (Ru → bpy; MLCT = metal-
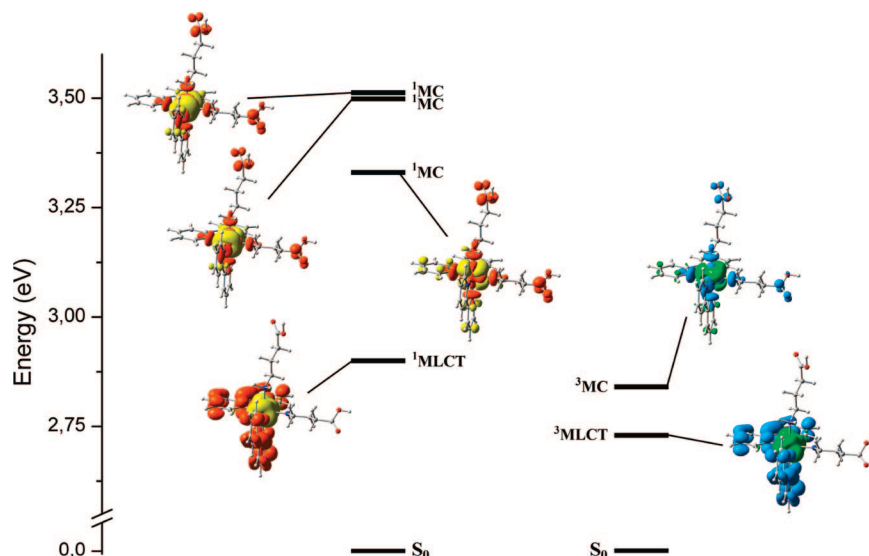
Figure 3. Selected singlet and triplet excited states of complex **4** with their respective electron density difference maps (EDDMs). Singlet EDDMs were obtained using the program GaussSum 1.05 (yellow indicates a decrease in charge density, while red indicates an increase). Triplet EDDMs were obtained using GaussView 4.1.2;[47] all major components and their relative weight were taken in consideration for each transition (green indicates a decrease in charge density, while blue indicates an increase).

to-ligand charge transfer) in all derivatives except **1**, which has ^{1}MLLCT (MLLCT = metal-ligand-to-ligand charge transfer) transitions due to 4ap contributions (Table 2). Two main ^{1}MLCT or ^{1}MLLCT transitions compose this low-energy band in **1** and **2**, but only one ^{1}MLCT transition is present in both **3** and **4**. Other ^{1}MLCT transitions are found at lower energy in the computed data, but they have very low oscillator strength values. In the experimental spectra of all complexes, a shoulder occurs at about 320 nm. The band is less prominent for **1** and **2** and is more evident for **3** and **4**. Ru → L MLCT states are responsible for these transitions; TDDFT calculations overestimate their energy in the case of **1** and **2**. In their simulated spectra, in fact, the shoulder is buried under the intense band at 280−300 nm. This last UV band is due to high-energy ^{1}MLCT states (Ru → bpy) for **1** and **2** and to $\pi-\pi^*$ states (bpy-centered) for **3** and **4**. It is worth highlighting that all derivatives have a group of ^{1}MC states above the main ^{1}MLCTs (Figure 3). These states play a crucial role in the photochemistry of **1−4**, providing photodissociation pathways (see below).

Emission Properties and Triplet Excited States of Complexes 1−4. Eight triplet excited-state energies for **1−4** were calculated from the ground-state geometries (**S1−4**) by TDDFT, as described in the Computational Details. As expected, the computed triplet states fall in a smaller energy range than the singlets. As shown for complex **4** in Figure 3, it was possible to find ^{3}MLCT transitions that have orbital composition in agreement with major ^{1}MLCT transitions (i.e., high oscillator strength values). The emission of **1−4** can be ascribed to ^{3}MLCT transitions at lower energy that can be populated from the first ^{3}MLCT after efficient intersystem crossing (ISC) with the main ^{1}MLCT state. TDDFT from **S1−4** geometries over-estimates the energy of the lowest-lying ^{3}MLCTs (**1**, 2.45 eV, 506 nm; **2**, 2.59 eV, 479 nm; **3**, 2.40 eV, 516 nm; and **4**, 2.43 eV, 510 nm).[7] For all of the complexes, a ^{3}MC state with dissociative character is close in energy to the ^{3}MLCTs. The other two dissociative ^{1}MC states found have higher energy and do not fall in proximity to the low-lying ^{3}MC.

Different results were obtained using the unrestricted Kohn−Sham method (UKS) for the determination of the
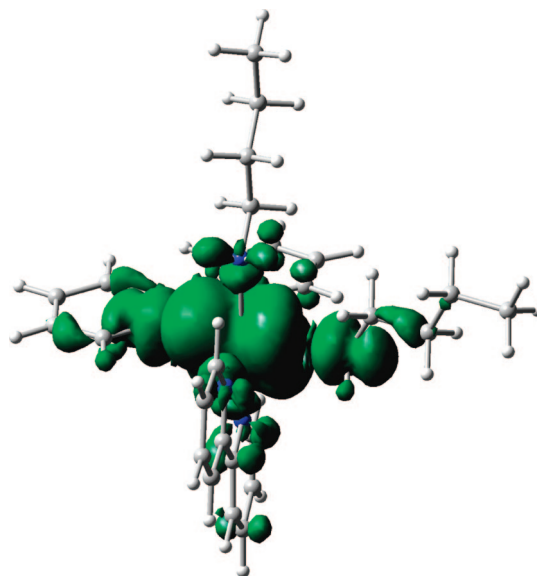

Figure 4. Countour plots of the spin density of the lowest-lying triplet state geometry of complex **3** (isovalue = 0.001).

electronic structure of the lowest-lying triplets (**T1−4**). As shown by the spin density surface of complex **3** (Figure 4), the lowest-lying triplets are all ^{3}MC states; electron density is mostly localized on the metal center and on the σ-orbitals of one butylamine ligand and of the pyridine ring *trans* to it. The differences in geometric parameters can explain the substantial differences between TDDFT and UKS results. In fact, ΔSCF energies of **1−4** calculated from **T1−4** geometries give values in the range 0.72−0.97 eV (1727−1281 nm) in the gas phase and 0.67−0.84 eV (1858−1467 nm) in solution. A better estimate of emission energies was obtained by calculating triplet states using TDDFT at the **T1−4** geometries. Complexes **1**, **3**, and **4** display a low-lying triplet state with ^{3}MLCT character at 1.58 eV (783 nm), 1.78 eV (696 nm), and 1.77 eV (701 nm), respectively. Unlike the other derivatives, a pure dissociative ^{3}MC is the lowest-lying state in **2**; its energy is 1.21 eV (1023 nm) higher than in the ground state. Theoretical energies

obtained with this set of calculations are in good agreement with experimental data (less so in the case of **1**).[7,50]

Photodissociation. Clues to the photodissociation mechanism and the dissociative excited states of **1**−**4** were obtained by elongating and selectively freezing the Ru−N5(L) bond (scheme in Table 1) and performing a TDDFT or UKS calculation after geometry relaxation. TDDFT calculations were performed for both singlet and triplet excited states. Transition energies and orbital compositions are reported in the Supporting Information.

In the singlet state, ^{1}MLCTs are separated from the set of three ^{1}MC states by 0.64 eV in **1**, 0.37 eV in **2**, 0.48 eV in **3**, and 0.43 eV in **4** (Figure 3). Along the Ru−N(L) stretching coordinate, no significant decrease of energy separations is observed for singlets. The ^{1}MLCT and ^{1}MC states remain distinct since no contributions from antibonding empty orbitals are found in the MLCTs. In fact, for short Ru−N(L) distances, the orbitals LUMO+10 or LUMO+11 of **1** and **2** and LUMO+6 or LUMO+7 of **3** and **4** are not significantly close in energy to the occupied orbitals and do not mix with other bpy-centered orbitals lying at lower energies. Mixing of orbitals occurs when long Ru−N(L) distances are reached (for example, at 2.58 Å in **2**). Normal-mode analysis shows that Ru−N(L) stretching allows bond elongation only in the 1.93−2.43 Å range, suggesting that dissociation from the singlet state is less probable since vibrations are not able to pull the LUMO+10 and LUMO+11 (or LUMO+6 and LUMO+7) close enough in energy to be populated. Such behavior accounts for the complexes' stability in the ground state in the absence of light.

In comparison to singlet states, the formation of triplet states upon light excitation and ISC produces different results along the Ru−N coordinate. In fact, a different scenario is obtained when triplet states are monitored along the same Ru−N(L) stretching coordinate. The energy separation between the ^{3}MLCT state(s) and the nearby ^{3}MC is significantly reduced with respect to that of the singlet state in all derivatives. A small energy gap between the ^{3}MLCT and ^{3}MC states is found already at the ground-state geometry. Furthermore, these energy gaps agree with the photodissociation yield trend **2** ≫ **3** ∼ **4** > **1**, being 0.06 eV for **2**, 0.11 eV for **3** and **4**, and 0.40 eV for **1**. The LUMO+10 of **1** and **2** and LUMO+6 of **3** and **4** contribute as the only virtual orbitals receiving electron density in the ^{3}MC states. With increasing Ru−N(L) distance, the antibonding orbitals LUMO+10 or LUMO+6 are stabilized and rapidly become more accessible for population from the occupied orbitals. Figure 5 shows LUMO+10 as the only empty orbital that is considerably lowers in energy upon Ru−N5(L) stretching in complex **2**. This orbital maintains its shape up to Ru−N(py) distances of 2.78 Å, despite partial mixing with ligand-centered orbitals. In contrast, the majority of the other orbitals show an increase in energy; among them is the other antibonding orbital, LUMO+11, which does not change its shape along the reaction coordinate.

In all complexes but **1**, an increase in the contribution from the antibonding orbitals is observed in the lowest-energy ^{3}MLCT triplets upon bond elongation. In **2** for example, the ^{3}MC is completely mixed with lower-energy ^{3}MLCTs already at Ru−N5(py) distances of 2.28 Å, when the Ru−N5(py) bond is just 0.1 Å from the ground-state equilibrium geometry. At this Ru−N5(py) distance, no pure ^{3}MC with dissociative character is present, since contributions from the LUMO+10 are dispersed

(50) Nikolenko, V.; Yuste, R.; Zayat, L.; Baraldo, L. M.; Etchenique, R. *Chem. Commun.* **2005**, 1752−1754.
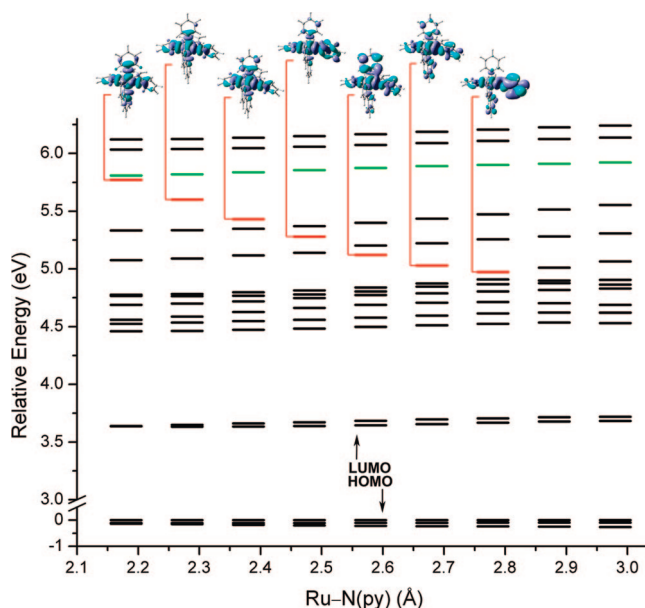

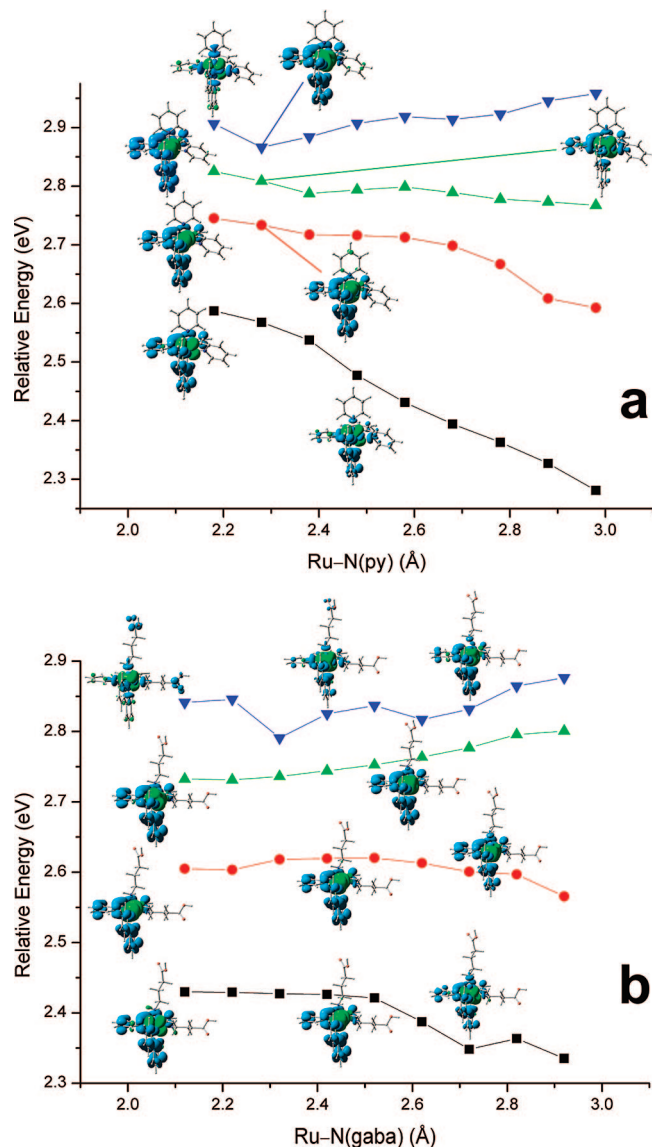***Figure 5.*** Orbital diagram evolution of the triplet electronic structure for **2** along the Ru−N(L) stretching coordinate; the red bar represents the LUMO+10, the green bar the LUMO+11.

among other ^{3}MLCT states. Furthermore, the emitting ^{3}MLCT (or what remains of it) is at higher energy. Similar behavior is found for **3** and **4**, but relevant differences are evident. In **3**, after 0.1 Å, the dissociative ^{3}MC is 50% mixed with the emitting ^{3}MLCT, while in **4**, the two states do not mix until the bond is elongated 0.3 Å. The different contributions of the LUMO+10 or LUMO+6 antibonding orbitals in low-energy MLCTs may explain the marked difference in the photodissociation yield of **2** with respect to the other derivatives. Complex **1** does not show any contribution from LUMO+10 in the lowest-lying triplet but exhibits a pure dissociative state 0.40 eV above the closest ^{3}MLLCT state. Only minor contributions (<10%) from LUMO+10 and LUMO+11 are present in the ^{3}MLLCT states of **1**, in agreement with its lower photodissociation yield.

Triplet excited-state evolution along the Ru−N(L) stretching coordinate was also tracked by analysis of ^{3}MC and ^{3}MLCT transition mixing. EDDMs obtained by TDDFT triplet calculations were employed for this task. Figure 6 describes the energy profiles of **2** and **4** for the dissociative ^{3}MC and a series of ^{3}MLCT states lying at lower energy. The evolution of the triplet excited-state character shows how the ^{3}MC mixes with ^{3}MLCTs and partially transfers to them its dissociative character. Mixing of ^{3}MC/^{3}MLCT characters occurs readily at 0.1 Å after the Ru−N(L) equilibrium distance for **2**, while only at 2.42 Å afterward is there significant mixing for **4**. In **2**, the lowest ^{3}MLCT has completely changed in a ^{3}MC at 2.48 Å. ^{3}MC/^{3}MLCT mixing is efficient in complex **3**, although the ^{3}MLCT states involved are at higher energy compared to **2**. In complex **1**, character mixing is smaller than in **2**−**4**. It is worth noting that such ^{3}MC/^{3}MLCT mixing can cause population of the ^{3}MC directly from the ^{1}MLCT state. This might explain why **2** is not emissive and has the highest dissociation yield (see below).

The UKS triplet geometry is consistent with the scenario described by TDDFT calculations of triplet states. The Ru−N5(L) bonds are longer in **T1**−**4** as a result of stabilization of the antibonding orbital LUMO+10 (**1** and **2**) or LUMO+6 (**3** and **4**). There is good correlation between Ru−N(L) bond lengths and the measured photodissociation yield of **1**−**4**, confirming
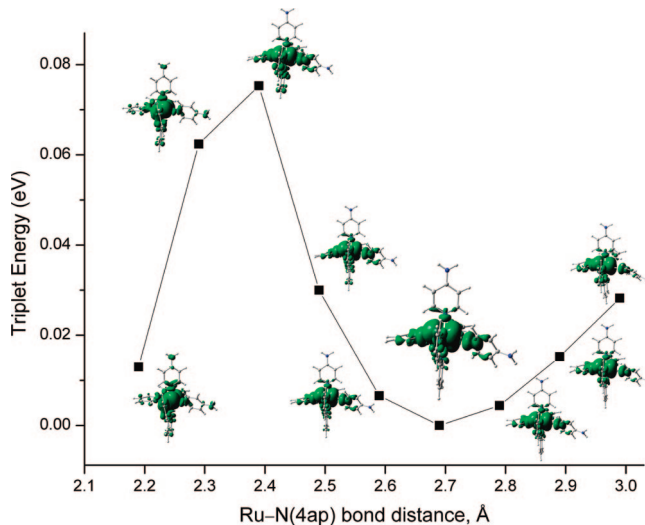
Figure 7. Potential energy curves of the lowest-lying triplet state of **1** along the Ru−N(4ap) coordinate (calculation performed with the UKS method). The zero-point of the energy scale is set to the triplet energy at **T1** (equilibrium) geometry.

the ^{3}MLCTs calculated by TDDFT). The energy profile in Figure 7 shows the considerable ^{3}MC energy changes along the coordinate for complex **1**. Shortening of Ru−N(L) bonds in **T1−4** causes important distortions in the octahedral geometry of the complexes. This fact may indicate that once ISC occurs, the progression toward the Ru−N(L) bond dissociation is favored by geometry relaxation. The UKS potential energy curve for the lowest-lying triplet of **2** is different from those of the other complexes (see Supporting Information). In fact, only one minimum is present in the curve of **2**, while a second minimum is present for short Ru−N(L) distances in **1**, **3**, and **4**. The presence of this second minimum may represent a sort of activation energy in the photodissociation of the first mono-dentate ligand for **1**, **3**, and **4**.

The electron density and electrostatic potential (ESP) surfaces were analyzed at different isovalues for all complexes in both the ground and triplet states. Figure 8 shows the ESP surface mapped over the electron density for **S4** and **T4**. There is no electron density between the ruthenium center and N5 in **T4**. Indeed, such a difference with **S4** can explain the weak interaction between the metal and the gaba ligand in the triplet state. The N1−bpy ring is detached from the Ru, but dissociation of bpy is prevented by the strong coordination of the other ring. It is also worth pointing out the increased charge (ESP) on N1 and N5 and the substantial decrease of charge on the ruthenium; both are in agreement with the shift of an electron from a purely metal-based orbital (Ru d-orbital) to the LUMO+6 (LUMO+10 for **1** and **2**), which has a significant σ-contribution from the two nitrogen atoms. Ligands with better π-acceptor properties can increase the photodissociation quantum yield by favoring the transfer of electron density from the metal to the σ-orbital centered on the nitrogen of the monodentate ligand.

Conclusions

The close proximity of the ^{3}MLCT and ^{3}MC states in the TDDFT scheme does not allow unequivocal establishment of the lowest-energy state for the ground-state geometry, at least for **2−4**. Nevertheless, the fluorescence of **1**, **3**, and **4** indicates that the lowest-lying state can be considered ^{3}MLCT. The absence of room-temperature emission in **2** suggests, in contrast, that the lowest-

Figure 6. Potential energy curves of the triplet excited states of **2** (a) and **4** (b) along the Ru−N(L) stretching coordinate. The zero-point of the energy scale is set to the ground-state energy at its equilibrium geometry. Selected EDDMS are presented in order to show the change in character of triplet excited states.

that **2** is the most efficiently dissociated ($\phi = 0.2$),[3] followed by **3** and **4** ($\phi = 0.04$)[7] and **1** ($\phi = 0.02$).[9] In fact, LUMO+10 (**1** and **2**) and LUMO+6 (**3** and **4**) are very similar to the high-energy SOMOs for all complexes in **T1−4**.

Scans of the UKS triplet energy were performed on **T1−4** where the Ru−N(L) distance was shifted and then frozen, allowing relaxation of the whole structure. Ru−N(L) distance changes do not cause any mixing in the orbital diagram. The high-energy SOMO remains antibonding and almost identical in shape along the whole coordinate. Only at the extremes of the axis does the SOMO undergo a slight change in shape. For example, in **4**, the main component of the SOMO orbital (metal d-orbital) is rotated 90°, which may account for the rotation of the monodentate ligand previously described. No crossing of the high-energy SOMO with empty bpy-centered orbitals occurs along the stretching coordinate, because the energy gap is too high. Indeed, this fact indicates that the ^{3}MC state is highly dependent on the Ru−N(L) distance, while ^{3}MLCTs are clearly less dependent (also confirmed by the small energy changes in
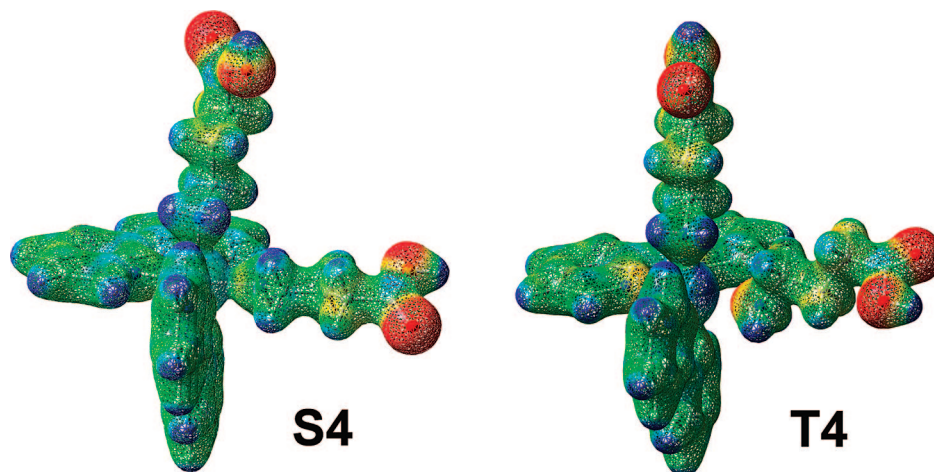
Figure 8. Electrostatic potential surface of complex **4** in the **S4** and **T4** states. ESP surfaces are shown both in space (with positive and negative regions shown in blue and red, respectively) and mapped on electron densities (isovalue = 0.05) of the molecule (ESP color scale is such that $\delta^+ \rightarrow \delta^-$ in the direction blue → green → yellow → orange → red).

lying triplet is ³MC. The trend in the energy gap between the ³MLCT and ³MC states agrees with the experimental photodissociation yield. The UKS triplet calculations clearly indicate that all derivatives have a ³MC lowest-lying triplet with remarkable dissociation character (as is apparent also from the long Ru−N(L) bonds). Intersystem crossing and the formation of a triplet state seem to be necessary for the dissociation of a monodentate ligand, since the antibonding orbitals, and thus the ¹MC states, are at an energy too high to be significantly affected by Ru−N(L) stretching. In contrast, carbonyl-containing metal complexes can dissociate CO ligands from the singlet state with a similar mechanism.[25–27,49,51,52]

A reasonable scenario for the photodissociation pathway, based on combined TDDFT and UKS results, can be described as follows: absorption of a photon triggers promotion of **1−4** to ¹MLCT states, which evolve efficiently to ³MLCT through ISC. Once the ³MLCTs are populated, they can decay radiatively, as observed experimentally for **1**, **3**, and **4**, and eventually relax vibrationally through quasi-dissociative ³MC states and reach the ground-state after ISC. The presence of such states in **1**, **3**, and **4** is described by TDDFT triplet calculations using **T1**, **T3**, and **T4** and can be foreseen from the presence of a second minimum in energy due to a different ³MC state in the potential energy surface (Figure 7 for **1**).

Simultaneously, mixing between ³MLCT and ³MC with dissociative character takes place after ISC upon geometry relaxation of the complexes (and maybe activation in the cases of **1**, **3**, and **4**). In this way, the dissociative ³MC can be progressively stabilized by Ru−N(L) bond stretching. The magnitude of the energy differences of the ³MC states along the Ru−N(L) stretching coordinate is consistent with this picture. According to DFT calculations, Ru−N(L) stretching mode causes oscillations in the 2.34−3.22 Å range for triplets (complex **2**). Therefore, direct population of the dissociative state (or heavily mixed ones) occurs from the singlet state when the molecule is hit by a proper photon, causing photodissociation of one monodentate ligand. In fact, temperature-dependent lifetime experiments on Ru−polypyridine complexes suggest

that ³MC states can be directly populated from ¹MLCT states.[3,53] Despite ³MC/³MLCT mixing and stabilization of the dissociative ³MC along the Ru−N(L) stretching coordinate, **1**, **3**, and **4** are still able to fluoresce, because populated pure ³MLCT can decay radiatively to the ground state. As a result, there is a decrease in the photodissociation yields of these derivatives. Complex **2** cannot emit, since the ³MC/³MLCT mixing is so efficient that pure ³MLCTs are present only at higher energies and cannot decay to ground state without populating dissociative states.

DFT and TDDFT are powerful tools that enable thorough investigation of electronic structure evolution over time. Access to such information is fundamental for a rational design of new photoactivable metal species with tunable photochemical features. Only a correct description of orbital energies and shapes, and a full comprehension of the role played by different excited states in light-induced electronic transitions, can guide the introduction of advantageous structural changes on model molecules.

Supporting Information Available: Frontier orbital diagrams for **1−4**; isodensity plots of the HOMO and LUMO for **1−4**, the two antibonding molecular orbitals for **1−4**, and the higher-energy SOMOs for **1**, **3** and **4**; calculated triplet excited states along the Ru−N(L) stretching coordinate for **1−4**; EDDMs of selected singlet and triplet excited states for **1−3**; potential energy curves of the lowest-lying triplet state along the Ru−N(L) stretching coordinate for **2−4**; orbital diagram evolution of the triplet electronic structure along the Ru−N(L) stretching coordinate for **1**, **3**, and **4**; electron density and electrostatic potential surfaces for **1−3**; and complete ref 33. This material is available free of charge via the Internet at http://pubs.acs.org.

JA8025906

(51) Farrell, I. R.; Matousek, P.; Vlček, A. *J. Am. Chem. Soc.* **1999**, *121*, 5296–5301.

(52) Víchová, J.; Hartl, F.; Vlček, A. *J. Am. Chem. Soc.* **1992**, *114*, 10903–10910.

(53) Meyer, T. J. *Pure Appl. Chem.* **1986**, *58*, 1193–1206.

(54) O'Boyle, N. M.; Tenderholt, A. L.; Langner, K. M. *J. Comput. Chem.* **2008**, *29*, 839–845.